



## OPEN ACCESS

## EDITED BY

Myrto K. Moutafi,  
University General Hospital Attikon, Greece

## REVIEWED BY

Xiaopan Xu,  
Air Force Medical University, China  
Jing Wang,  
Mass General Brigham, United States

## \*CORRESPONDENCE

Yi-Kai Xu

✉ yikai.xu@163.com

Jiancheng Yang

✉ jiancheng.yang@epfl.ch

Jun Xu

✉ 188352165@qq.com

<sup>†</sup>These authors have contributed equally to this work

RECEIVED 14 July 2024

ACCEPTED 25 October 2024

PUBLISHED 15 November 2024

## CITATION

Hao P, Yu Y, Huang C-T, Zhou F, Xu Y-K, Yang J and Xu J (2024) Advancing EGFR mutation subtypes prediction in NSCLC by combining 3D pretrained ConvNeXt, radiomics, and clinical features. *Front. Oncol.* 14:1464555. doi: 10.3389/fonc.2024.1464555

## COPYRIGHT

© 2024 Hao, Yu, Huang, Zhou, Xu, Yang and Xu. This is an open-access article distributed under the terms of the [Creative Commons Attribution License \(CC BY\)](https://creativecommons.org/licenses/by/4.0/). The use, distribution or reproduction in other forums is permitted, provided the original author(s) and the copyright owner(s) are credited and that the original publication in this journal is cited, in accordance with accepted academic practice. No use, distribution or reproduction is permitted which does not comply with these terms.

# Advancing EGFR mutation subtypes prediction in NSCLC by combining 3D pretrained ConvNeXt, radiomics, and clinical features

Peng Hao<sup>1†</sup>, Yinghong Yu<sup>2†</sup>, Chan-Tao Huang<sup>1</sup>, Fang Zhou<sup>1</sup>, Yi-Kai Xu<sup>1\*</sup>, Jiancheng Yang<sup>2,3\*</sup> and Jun Xu<sup>4\*</sup>

<sup>1</sup>Department of Diagnostic Imaging Center, Nanfang Hospital, Southern Medical University, Guangzhou, Guangdong, China, <sup>2</sup>Algorithm Department, Dianei Technology, Shanghai, China, <sup>3</sup>Computer Vision Laboratory, Swiss Federal Institute of Technology Lausanne (EPFL), Lausanne, Switzerland, <sup>4</sup>Department of Hematology, Nanfang Hospital, Southern Medical University, Guangzhou, Guangdong, China

**Purpose:** The aim of this study was to develop a novel approach for predicting the expression status of Epidermal Growth Factor Receptor (EGFR) and its subtypes in patients with Non-Small Cell Lung Cancer (NSCLC) using a Three-Dimensional Convolutional Neural Network (3D-CNN) ConvNeXt, radiomics features and clinical features.

**Materials and methods:** A total of 732 NSCLC patients with available CT imaging and EGFR expression data were included in this retrospective study. The region of interest (ROI) was manually segmented, and clinicopathological features were collected. Radiomic and deep learning features were extracted. The instances were randomly divided into training, validation, and test sets. Feature selection was performed, and XGBoost was used to create solo models and combined models to predict the presence of EGFR and subtypes mutations. The effectiveness of the models was assessed using ROC and PRC curves.

**Results:** We established the following models: Model<sub>CNN</sub>, Model<sub>radiomic</sub>, Model<sub>clinical</sub>, Model<sub>CNN+radiomic</sub>, Model<sub>CNN+clinical</sub>, Model<sub>radiomic+clinical</sub>, and Model<sub>CNN+radiomic+clinical</sub>, which were based on deep learning features, radiomic features, clinical data and combinations of these, respectively. In predicting EGFR mutations, Model<sub>CNN+radiomic+clinical</sub> demonstrated superior performance compared to other prediction models, achieving an AUC of 0.801. For distinguishing between EGFR subtypes ex19del and L858R, Model<sub>CNN+radiomic</sub> reached the highest AUC value of 0.775.

**Conclusions:** Both deep learning models and radiomic signature-based models offer reasonably accurate non-invasive predictions of EGFR status and its subtypes. Fusion models hold the potential to enhance noninvasive methods for predicting EGFR mutations and subtypes, presenting a more reliable prediction approach.

## KEYWORDS

NSCLC, EGFR, CT, deep learning, radiomic

## Introduction

Lung cancer stands as the most lethal form of cancer globally, presenting the highest mortality rate among all malignancies. Approximately 80% of lung cancers belong to the histological category of non-small-cell lung cancer (NSCLC) (1). Currently, clinical treatment for lung cancer focuses on controlling local lesions and metastases. Targeted therapy offers advantages such as precise targeting, minimal side effects, ease of use, and high therapeutic efficacy (2).

One of the key proteins involved in lung cancer is the epidermal growth factor receptor (EGFR). Lung cancer can be classified into two categories: EGFR mutation-positive tumors and non-mutated tumors (EGFR wild type) (3). The EGFR ex19 Del and L858R mutations account for 90% of EGFR mutation-positive cases and affect approximately 50% of individuals with lung adenocarcinoma in the Asian population. Patients with wild-type EGFR cannot benefit from EGFR-tyrosine kinase inhibitor (TKI) treatment (4). Studies have shown that patients with EGFR ex19del mutation have better prognosis and treatment response compared to those with L858R mutation. For instance, in the context of osimertinib combination therapy or osimertinib targeted therapy alone, patients with EGFR ex19del mutation have shown longer progression-free survival (PFS) compared to those with L858R mutation (5). Therefore, accurately defining the EGFR mutation subgroups can be crucial in ensuring precise diagnosis and individualized treatment for NSCLC patients. The accuracy of EGFR gene assessment using biopsy samples may be compromised due to significant intratumor heterogeneity. Additionally, some patients may have inoperable lung adenocarcinoma or may not be able to undergo biopsy due to factors such as endurance, willingness, or cost. Therefore, a non-invasive approach to determine EGFR mutation status and subtypes is needed. Computer tomography (CT) is commonly used for lung cancer diagnosis. Machine learning (ML) and artificial intelligence can thoroughly evaluate tumors, improve the sensitivity and specificity of diagnostic imaging, and provide a non-invasive method for lung cancer-related diagnosis (6, 7). However, the aforementioned deep learning (DL) study only focused on identifying the presence of EGFR mutations (wild-type versus ex19Del+L858R), without specifically differentiating between the subtypes of EGFR mutations (ex19Del vs L858R), or only using machine learning (8–10).

In this study, we aimed to directly distinguish between EGFR (+) and EGFR (-) and then differentiate between two common subtypes of EGFR mutations, ex19Del and L858R, using DL and ML analysis of primary lung adenocarcinoma. The findings of this study may contribute to a more comprehensive and non-invasive discrimination of EGFR mutations and subtypes. This, in turn, could serve as a foundation for developing individually tailored and effective diagnosis and treatment plans for lung cancer patients.

## Materials and methods

### Patients inclusion

From May 2012 to August 2021, a retrospective study was conducted on all CT scans of non-small cell lung cancer (NSCLC)

patients from the Picture Archiving and Communication System (PACS) at Nanfang Hospital. A total of 1080 patients with pathologically proven lung cancer who underwent surgery or received biopsy were included in this study. The clinical features of the patients were retrieved from the hospital information system. Inclusion criteria for this study were: (1) patients with confirmed EGFR gene mutation status and pathological testing of tumor specimens; (2) patients with pretreatment CT images; (3) patients with complete clinical data (including sex, age, smoking, T stage, and lesion size). Exclusion criteria were: (1) patients who received treatment before CT scan; (2) patients with a time interval longer than one month between CT examination and treatment; (3) patients with multiple tumor nodules in the lung; and (4) patients with tumor lesions near the hilar that could not be separated from neighboring hilar architecture. Based on these criteria, a total of 732 patients were included in the study. The TNM system based on the American Joint Committee on Cancer (AJCC) manual was used for staging (11).

In this study, a total of 1080 cases were initially included. However, 348 cases were excluded for various reasons. These exclusions included cases without pre-treatment CT images (n=132), cases with multifocal primary tumors (n=70), cases where the time interval between biopsy or surgery was more than 12 weeks (n=50), cases with tumors in the mediastinum (n=10), cases with severe infection (n=10), and cases with mutations in exons 18 and 20 (n=16). The latter exclusion was due to the insufficient number of tumors with these specific mutations for reasonable statistical analysis.

The focus of this study was on mutations in exons 19del and L858R of the EGFR gene. After the exclusions, the final study cohort consisted of 732 patients. Among these patients, there were a total of 351 cases with EGFR mutations, with 195 cases of EGFR ex19del and 156 cases of EGFR L858R. This distribution represents approximately 55% of cases with EGFR ex19del and 45% of cases with EGFR L858R. For more detailed information on the distribution of cases and mutations, please refer to Tables 1, 2.

Among the patients included in the study, 351 out of 732 (48%) tested positive for an EGFR mutation, while 381 out of 732 (52%) tested negative for an EGFR mutation. We observed a significant association between EGFR mutations and non-smoking female patients with non-small cell lung cancer, as shown in Supplementary Table S1.

Out of the total cases with EGFR mutations, 195 (55%) were identified as EGFR Ex19del and 156 (45%) were identified as EGFR L858R. This distribution indicates that EGFR Ex19del is slightly

TABLE 1 Distribution of data for predicting EGFR mutations.

	Total	EGFR+	EGFR-
Total	732	351	381
Training group	512	246	266
Validation group	73	35	38
Testing group	147	70	77

EGFR (+), EGFR mutation-positive; EGFR (-), EGFR mutation-negative.

TABLE 2 Distribution of data for distinguishing EGFR ex19del from L858R.

	Total	EGFR ex19del	EGFR L858R
Total	351	195	156
Training group	245	136	109
Validation group	35	19	16
Testing group	71	40	31

more prevalent than L858R. Additionally, we found that the L858R mutation was associated with older patients, as indicated in Supplementary Table S2.

## CT scanning

The patients were examined using either a 256-slice iCT scanner (Philips Healthcare, Best, Netherlands) or Siemens Medical Solutions' Sensation 64 or Definition AS scanner (Forchheim, Germany). The scanning parameters for the two scanners were as follows: tube rotation time of 0.5 s, pitch of 0.87 or 1.2, detector collimation of 128 x 0.625 or 64, tube voltage of 120 kV, tube current of 100-300 mA, field view of 350 mm, matrix of 512x512, slice thickness of 1-5 mm, reconstruction interval of 1 mm.

## Histopathology and EGFR status determination

The histopathological type of non-small cell lung cancer was determined by diagnostic pathologists using the 2011 International and Multidisciplinary Classification and the criteria put forward by the World Health Organization (WHO) 2015 guidelines for lung cancer categorization and the International Association for the Study of Lung Cancer/American Thoracic Society/European Respiratory Society. The EGFR mutation status was determined using a real-time fluorescent PCR-based amplification refractory mutation system and a human EGFR gene mutation real-time reverse transcription-polymerase chain reaction diagnostic kit (AmoyDx, Xiamen, China). The mutation status of EGFR exons 18, 19, 20, and 21 was analyzed.

## Clinical information

We extracted five features from the clinical information, including sex, age, smoking, T stage, and lesion size. The clinical features of the patients were retrieved from the hospital information system.

## Radiomic analysis

We extracted 1051 radiomic features from the image ROI and corresponding ROI mask. We then used Boruta (12) for feature selection on the training dataset. Boruta operates on two principles:

shadow features and biological distribution. This algorithm autonomously conducts feature selection on the dataset.

To examine the differences in radiomics features between the EGFR mutation-positive EGFR (+) and EGFR mutation-negative EGFR (-) groups, we conducted feature selection with Boruta. The algorithm identified 11 radiomics. These selected features can potentially serve as predictive markers for EGFR mutations. Further analysis and validation are needed to confirm their significance and utility in clinical practice. Additionally, for the specific EGFR mutation subtypes (EGFR ex19del and L858R), we performed radiomics feature extraction and identified 9 radiomics (details in Supplementary Methods).

## Model for deep learning

Our research focuses on developing a deep learning framework for accurately predicting gene mutations in nodules. To achieve this, we utilized ConvNeXt, a powerful deep learning model that achieved top-1 accuracy on the ImageNet dataset in early 2022 (13). ConvNeXt is composed of standard convolutional modules and has demonstrated exceptional accuracy and scalability. For our experiments, we specifically used the ConvNeXt-B model, which consists of 89 million parameters (14, 15), the pipeline overview is shown in Figure 1. Acknowledging the three-dimensional nature of CT images, we utilized ACS conv (<https://github.com/M3DV/ACSCConv>) to convert a 2D pre-trained model based on ImageNet-22K into a 3D model (16). In our approach, we preprocessed the input images by cropping them around the nodule center with a size of 32x64x64 (64x64 pixels in the axial plane, 32 frames). We then upsampled the images by a factor of 2 to 64x128x128 before feeding them into the model. Features are extracted through downsampling until the size of the feature map becomes 2x4x4. Finally, we applied global average pooling to generate a 1024-dimensional feature vector for classification. For the gene mutation classification task, we employed a simple Multi-Layer Perceptron (MLP) with one hidden layer. This MLP takes the 1024-dimensional feature vector as input and performs the final classification. During our experiments, we randomly selected data for training, validation, and testing, with a ratio of 7:1:2. The validation dataset was used to select the best model, and we reported the test results on both the validation and test sets. The deep learning model was implemented with Python 3.8.12 and PyTorch 1.11.0.

## Feature fusion

In our research, we investigated four distinct strategies for feature integration. Each fusion method employed the use of XGBoost to construct the model (17). The initial fusion, termed as Model<sub>CNN+clinical</sub>, integrated deep learning features (specifically the predictive probability of ConvNeXt) with clinical data (sex, age, smoking history, T stage, and lesion size). The second fusion, identified as Model<sub>CNN+radiomic</sub>, merged deep learning features with radiomic characteristics. The third fusion, labeled as Model<sub>radiomic+clinical</sub>, combined radiomic attributes with clinical

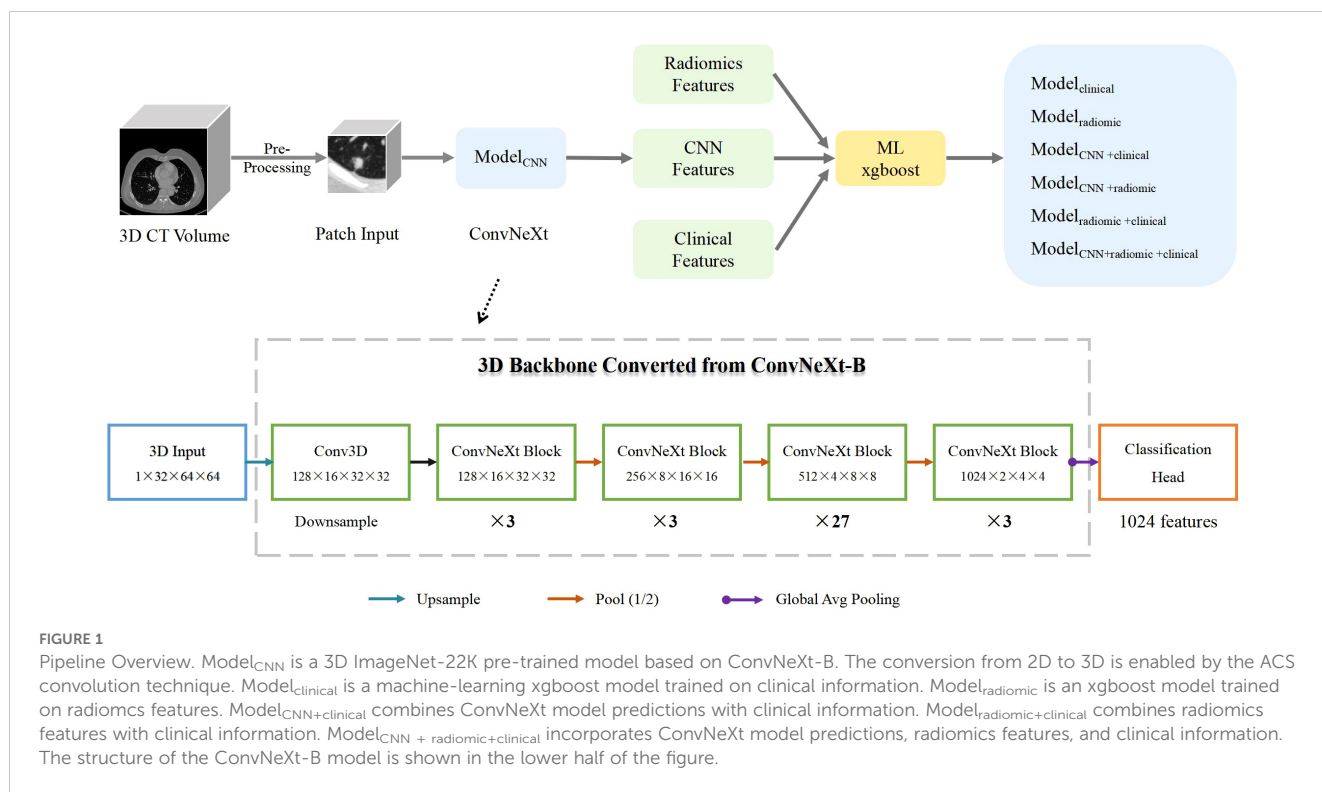


**FIGURE 1** Pipeline Overview. Model<sub>CNN</sub> is a 3D ImageNet-22K pre-trained model based on ConvNeXt-B. The conversion from 2D to 3D is enabled by the ACS convolution technique. Model<sub>clinical</sub> is a machine-learning xgboost model trained on clinical information. Model<sub>radiomic</sub> is an xgboost model trained on radiomics features. Model<sub>CNN+clinical</sub> combines ConvNeXt model predictions with clinical information. Model<sub>radiomic+clinical</sub> combines radiomics features with clinical information. Model<sub>CNN + radiomic+clinical</sub> incorporates ConvNeXt model predictions, radiomics features, and clinical information. The structure of the ConvNeXt-B model is shown in the lower half of the figure.

information. Lastly, the fourth fusion model, referred to as Model<sub>CNN+radiomic+clinical</sub>, amalgamated deep learning features, radiomics attributes, and clinical data. To evaluate the performance of these feature fusion approaches, we utilized ROC (Receiver Operating Characteristic) and PRC (Precision-Recall Curve) curves. These curves provide valuable insights into the model’s ability to discriminate between positive and negative cases, as well as its precision and recall. Accuracy, Recall, Precision, Specificity, and F1-score are calculated using the Youden index, which is defined as sensitivity + specificity – 1 (18).

### Statistical analysis

Statistical analysis was performed using IBM SPSS Statistics version 25.0. Continuous variables were analyzed using the two independent samples t-test or Mann-Whitney U test, depending on the distribution of the data. Categorical variables were analyzed using the chi-square test or Fisher’s exact test. The significance of

the ML model’s performance in differentiating between EGFR+ and EGFR- groups, as well as between ex19del and L858R mutations, was assessed using the same statistical methodologies.

## Results

### Performance in predicting EGFR mutation

We evaluated the performance of different models in predicting EGFR mutation status using the area under the curve (AUC) metric as presented in Table 3. In Table 3, pairwise DeLong tests were conducted between the first three columns (CNN, clinical, and radiomic models) and the last four columns (fusion models), yielding p<0.05. This indicates a significant difference in AUC between the multimodality fusion models and the single modality models. However, there were no significant differences between the single modality models (p>0.05), nor between the multimodality models themselves (p>0.05). In addition, Table 4 displays

**TABLE 3** AUC performance of different models for predicting EGFR mutations across the training, validation, and test sets.

AUC	Model CNN	Model clinical	Model radiomic	Model CNN+clinical	Model CNN+radiomic	Model radiomic+clinical	Model CNN+radiomic+clinical
Training	0.73	0.687	0.714	0.785	0.788	0.802	<b>0.81</b>
Validation	0.78	0.761	0.774	0.863	0.823	0.842	<b>0.848</b>
Testing	0.753	0.691	0.741	0.777	0.764	0.788	<b>0.801</b>

The best-performing value in each column is highlight in bold.

TABLE 4 Additional performance metrics of different models for predicting EGFR mutations in the testing set.

	AUC	Accuracy	Recall	Precision	Specificity	F1-score
Model <sub>CNN</sub>	0.753	<b>0.694</b>	0.743	<b>0.658</b>	0.649	<b>0.698</b>
Model <sub>clinical</sub>	0.691	0.646	0.757	0.602	0.545	0.671
Model <sub>radiomic</sub>	0.741	0.66	0.729	0.622	0.597	0.671
Model <sub>CNN+clinical</sub>	0.777	0.667	<b>0.786</b>	0.618	0.558	0.692
Model <sub>CNN+radiomic</sub>	0.764	0.68	0.7	0.653	<b>0.662</b>	0.676
Model <sub>radiomic+clinical</sub>	0.788	0.68	0.771	0.635	0.597	0.697
Model <sub>CNN+radiomic+clinical</sub>	<b>0.801</b>	0.68	0.757	0.639	0.61	0.693

The best-performing value in each column is highlight in bold.

supplementary performance metrics (including accuracy, recall, precision, specificity, and F1-score), while Figure 2 showcases the ROC and PRC curves. For the CNN probability prediction model, the AUC values were 0.73, 0.78, and 0.753 in the training, validation, and test groups, respectively. These results indicate that the CNN model has moderate predictive ability for EGFR mutation. To further improve the predictive performance, we developed a fusion model that combines deep learning, radiomics features, and clinical information. This model, called Model<sub>CNN + radiomic + clinical</sub>, achieved higher AUC values compared to the CNN model. Specifically, the AUC values for the fusion model were 0.81, 0.848, and 0.801 in the training, validation, and test groups, respectively. These results demonstrate that integrating multiple data sources can enhance the accuracy of EGFR mutation prediction. Overall, the fusion model shows promising performance in predicting EGFR mutation status and may have potential clinical utility in guiding treatment decisions for non-small cell lung cancer patients.

### Performance in distinguishing EGFR Ex19del and L858R mutations

We assessed various models' efficacy in distinguishing between EGFR Ex19del and L858R mutations, with AUC detailed in Table 5. Additionally, Table 6 presents supplementary performance metrics, and Figure 3 illustrates the ROC and PRC curves. For the deep learning model, the AUC values were 0.781, 0.765, and 0.751 in the training, validation, and test groups, respectively. These results indicate that the deep learning model has moderate predictive ability for distinguishing between these two mutation types. To further improve the performance, we developed a fusion model called Model<sub>CNN+radiomic</sub>. This model combines deep learning with radiomics features and has shown improved predictive performance. Specifically, the fusion model achieved AUC values of 0.811 in the validation group and 0.775 in the test group. These results suggest that the fusion model is better at distinguishing

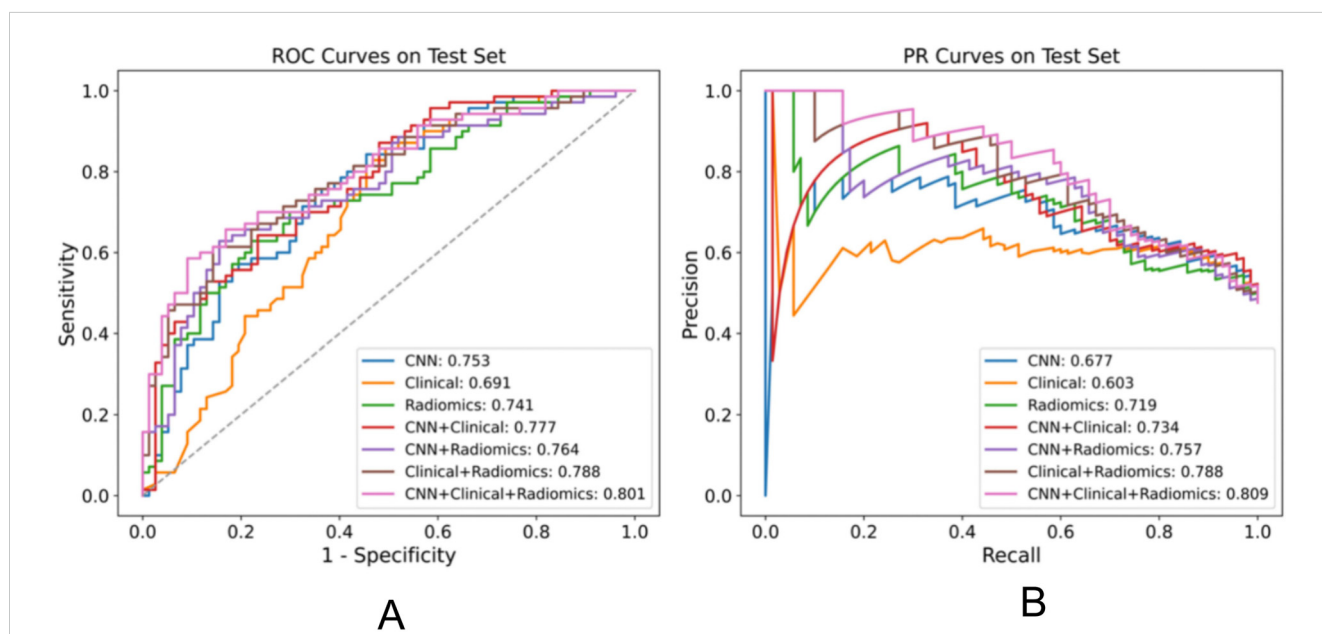


FIGURE 2 Performance comparison of various models for the EGFR mutation task on the test set, displaying the AUC for each model in the legend. (A) ROC plot (B) PR plot.



TABLE 5 AUC performance of different models for distinguishing ex19del, L858R across the training, validation, and test sets.

AUC	Model CNN	Model clinical	Model radiomic	Model CNN+clinical	Model CNN+radiomic	Model radiomic+clinical	Model CNN+radiomic+clinical
Training	0.781	0.613	0.733	0.767	0.775	0.726	<b>0.793</b>
Validation	0.765	0.589	0.724	0.771	<b>0.811</b>	0.763	0.809
Testing	0.751	0.537	0.684	0.752	<b>0.775</b>	0.742	0.772

The best-performing value in each column is highlight in bold.

TABLE 6 Additional performance metrics of different models on distinguishing ex19del and L858R in the testing set.

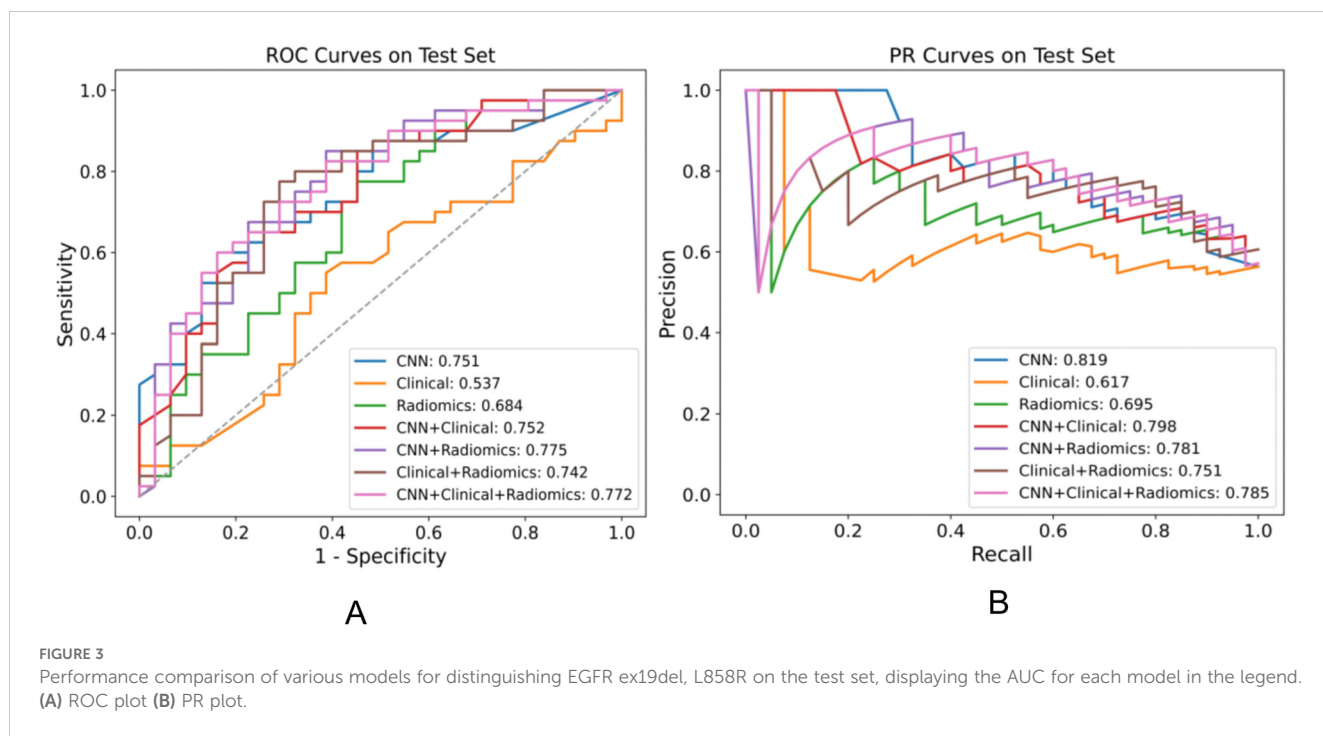
	AUC	Accuracy	Recall	Precision	Specificity	F1-score
Model <sub>CNN</sub>	0.751	<b>0.676</b>	<b>0.65</b>	0.743	0.71	<b>0.693</b>
Model <sub>clinical</sub>	0.537	0.535	0.425	0.63	0.677	0.507
Model <sub>radiomic</sub>	0.684	0.62	<b>0.65</b>	0.667	0.581	0.658
Model <sub>CNN+clinical</sub>	0.752	0.62	0.4	0.842	0.903	0.542
Model <sub>CNN+radiomic</sub>	<b>0.775</b>	0.648	0.525	0.778	0.806	0.627
Model <sub>radiomic+clinical</sub>	0.742	0.649	0.55	0.759	0.774	0.638
Model <sub>CNN+radiomic+clinical</sub>	0.772	0.577	0.3	<b>0.857</b>	<b>0.935</b>	0.444

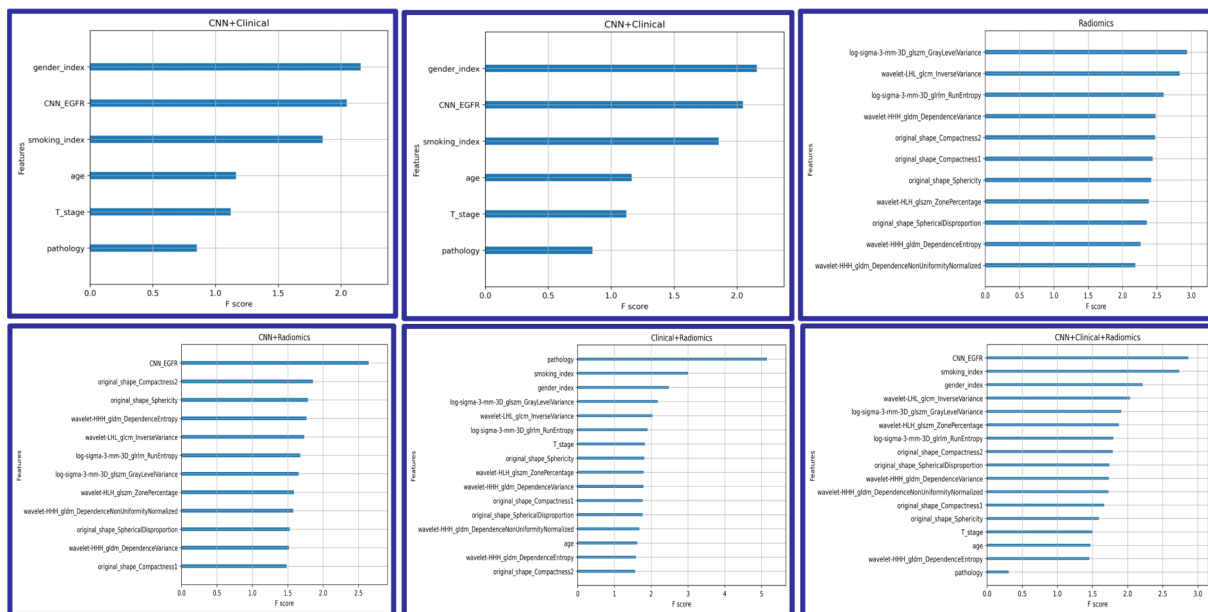
The best-performing value in each column is highlight in bold.

between EGFR Ex19del and L858R mutations compared to the deep learning model alone. Overall, our findings demonstrate that the fusion model, combining deep learning and radiomics features, has superior performance in accurately distinguishing between EGFR Ex19del and L858R mutations.

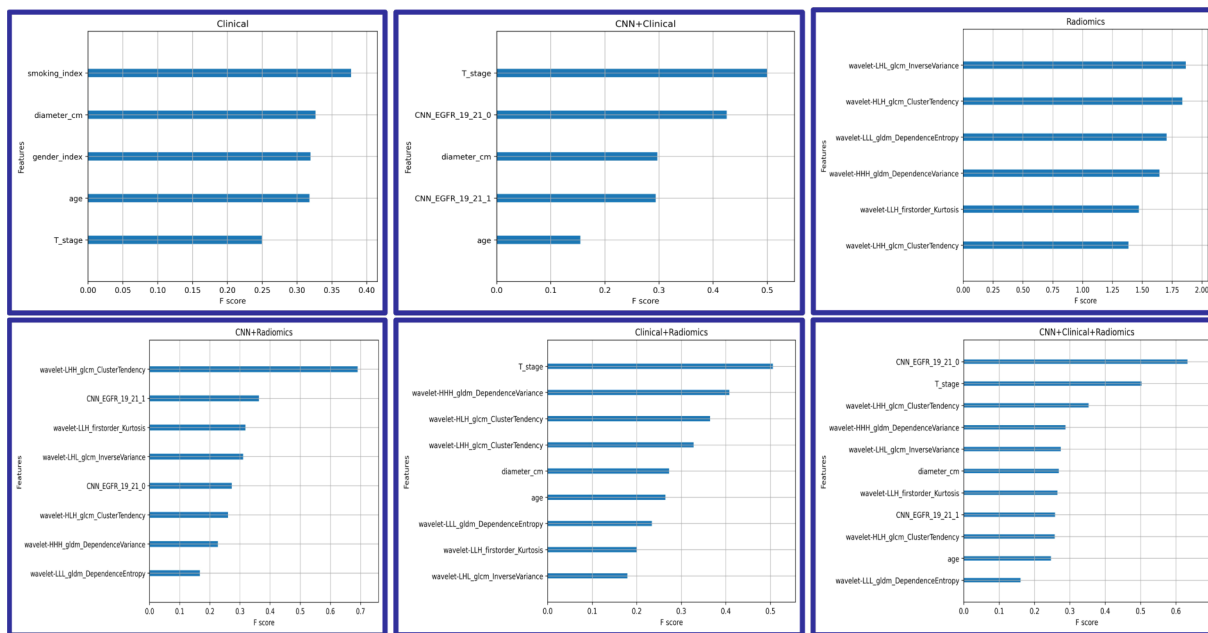
### Analysis of feature importance and cluster maps

The analysis of feature importance in the fusion model provides us with valuable insights, as depicted in Figure 4.





A



B

**FIGURE 4** Feature importance of Model<sub>clinical</sub>, Model<sub>radiomic</sub>, Model<sub>CNN+clinical</sub>, Model<sub>CNN+radiomic</sub>, Model<sub>radiomic+clinical</sub>, and Model<sub>CNN+radiomic+clinical</sub>. (A) Predicting EGFR mutations. (B) Distinguishing ex19del and L858R.

When discriminating EGFR mutations, in the CNN + radiomic + clinical fusion model, the most important features are the CNN extracted features, smoking index, and gender, followed by radiomic features. For discriminating EGFR Ex19del and L858R mutations, CNN and nodule size, along with radiomic features, are comparatively more significant.

To analyze the performance of the CNN-extracted features, we examined the clustering relationship between the 1024 CNN

features extracted by the model prior to classification and the labels in Figure 5. It can be observed that in both classification tasks, the unsupervised clusters of the 1024 deep-learned radiomics features extracted from ConvNext align closely with the semantic labels. In other words, the continuous regions on the black-grey bars share numerous similar features, respectively. Similarly, in Figure 6, across both tasks, we also observed a rather good clustering relationship between the fusion of CNN features,

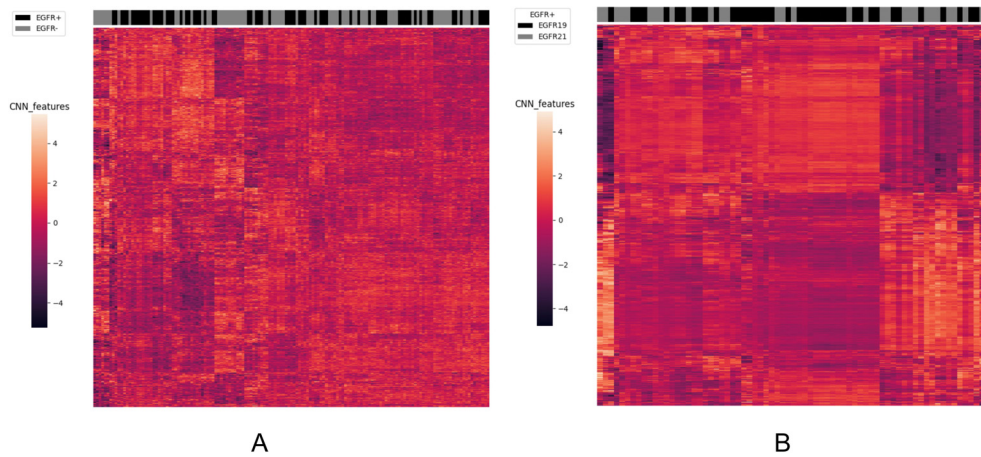


**FIGURE 5**  
 The clustering relationship of ConvNeXt features extracted by the model. **(A)** In the task of predicting EGFR mutations, the x-axis represents 147 nodules from the test set, and the y-axis represents the 1024-dimensional features extracted by CNN. Each feature has been normalized. Nodules within the same cluster (adjacent columns) exhibit similar radiomics characteristics in Euclidean space. The black gray bar indicates the semantic tag EGFR +/- for each nodule. **(B)** In the task of distinguishing ex19del and L858R, the x-axis represents 71 nodules from the test set, and the y-axis represents the 1024-dimensional features extracted by CNN. Again, each feature has been normalized. Nodules within the same cluster exhibit similar radiomics characteristics, and the black gray bar indicates the semantic label EGFR ex19del/EGFR L858R for each nodule.

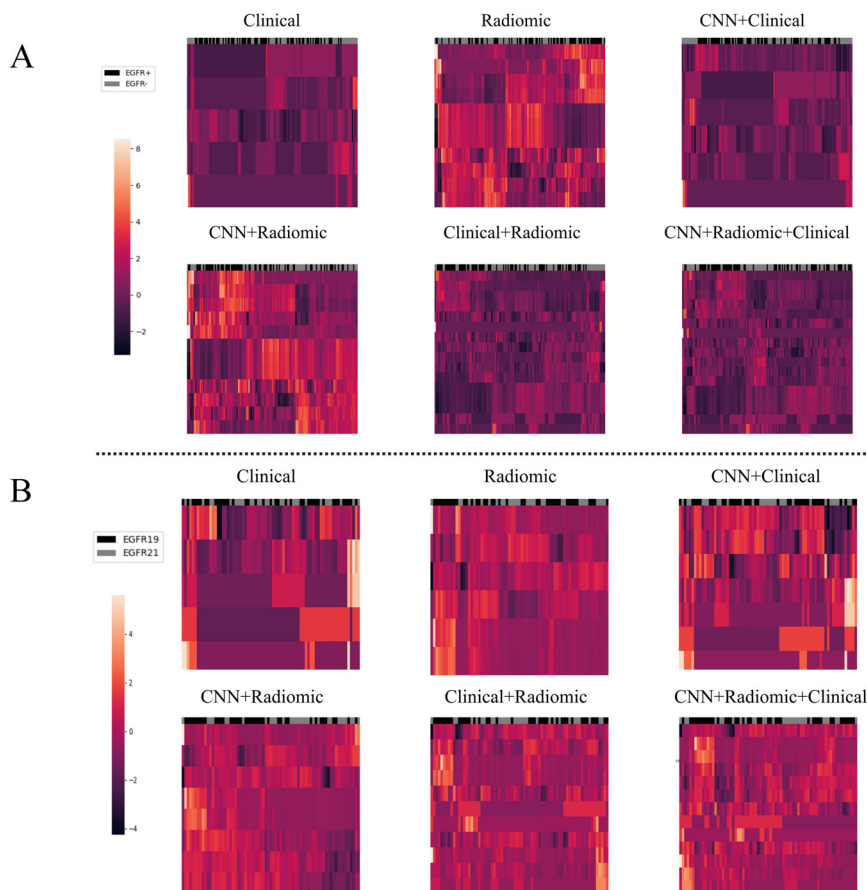


**FIGURE 6**  
 The clustering relationship of different models based on various features. **(A)** In the task of predicting EGFR mutations, the x-axis represents 147 nodules from the test set, and the y-axis represents the features of different models such as  $Model_{clinical}$ ,  $Model_{radiomic}$ ,  $Model_{CNN+clinical}$ ,  $Model_{CNN+radiomic}$ ,  $Model_{radiomic+clinical}$ , and  $Model_{CNN+radiomic+clinical}$ . Each feature has been normalized. Nodules in the same cluster (adjacent columns) have similar radiomic characteristics in Euclidean space. The black gray bar indicates the semantic tag EGFR +/- for each nodule. **(B)** In the task of distinguishing ex19del and L858R, the x-axis represents 71 nodules from the test set, and the y-axis represents the features of the different models. Again, each feature has been normalized. Nodules in the same cluster have similar radiomic characteristics, and the black gray bar indicates the semantic label EGFR ex19del/EGFR L858R for each nodule.



clinical features, radiomics features, and the labels. This suggests that the features we extracted possess a certain discriminatory ability and exhibit improved diagnostic performance after fusion.

## Discussion

In this study, we aimed to develop a fusion model that combines clinical, radiomic, and deep learning data to predict EGFR mutation subtypes in non-small cell lung cancer (NSCLC) patients. Compared to models based solely on radiomic or deep learning features, our fusion model (Model<sub>CNN+radiomic+clinical</sub>) demonstrated superior effectiveness. Previous studies have primarily focused on using deep learning approaches to predict the overall EGFR mutation status without clearly distinguishing between different mutation subtypes (6, 19). Zhao et al. developed a deep learning system based on 3D CNNs to automatically predict EGFR mutant pulmonary adenocarcinoma in CT images, with AUCs of 75.8% and 75.0% for holdout test set and public test set, respectively (20). However, the analysis did not cover EGFR mutation subtypes. In earlier investigations, Liu et al. only employed radiomics characteristics predicted the overall EGFR mutation status (wild-type vs 19DEL + L858R), and then discriminated between EGFR 19DEL and L858R (19DEL vs L858R), with AUCs of 0.76, 0.70, and 0.66, respectively (20). Song et al. employed DL to predict the mutation statuses of the EGFR (wild-type vs. 19DEL + L858R), 19DEL (19Del vs. wild-type + L858R), and L858R (L858R vs. wild-type + 19Del) with the AUC value 0.79 and 0.62, respectively (8). However, it is important to note that patients with EGFR Ex19del and L858R mutations exhibit significant differences in treatment response and prognosis (21). Radiomics quantifies medical images into multiple features and correlates them with gene characteristics (22). In contrast, Convolutional Neural Networks (CNN) evaluate image features at different levels. Deep Learning (DL) has advantages over radiomics as it learns complex features without manual delineation, can perform end-to-end tasks, and optimizes the loss function for better classification. DL outperforms radiomics in predicting EGFR mutations in lung cancer and has advantages in gene prediction for other cancers (23). In our study, we have developed a hybrid system that combines deep learning models with radiomics features. This strategy harnesses the pattern recognition capabilities of deep learning and the interpretability of radiomics features obtained through feature engineering. Our model has demonstrated superior performance, with higher AUC compared to only use machine learning or DL models. This approach showcases the synergy of combining these two techniques, resulting in improved results.

However, it is important to acknowledge the limitations of our study. Firstly, the generalizability of our findings may be limited as all patients were from the same center. Future studies should include data from multiple centers and diverse ethnicities to validate the results. Secondly, our study focused on NSCLC patients with non-small lung cancer, and the results may not be applicable to other histological subtypes. Finally, the radiomics-based approach requires precise labeling of tumor boundaries and processing of raw data, which can be time-consuming.

In future studies, it would be beneficial to collect data from multiethnic patient populations and multiple centers to enhance the generalizability of the findings. Additionally, an end-to-end approach that includes automatic tumor recognition, localization, and EGFR mutation prediction can be developed. Integrating radiomics features into deep learning models, along with clinical features and multi-level features, can further improve prediction performance. The resulting models can aid in determining appropriate EGFR-TKI therapy options for NSCLC patients in a non-invasive, reproducible, and cost-effective manner.

## Data availability statement

The original contributions presented in the study are included in the article/[Supplementary Material](#). Further inquiries can be directed to the corresponding author.

## Ethics statement

The studies involving humans were approved by Ethical Committee of the Nanfang Hospital. The studies were conducted in accordance with the local legislation and institutional requirements. Written informed consent for participation was not required from the participants or the participants' legal guardians/next of kin because Retrospective studies do not require written informed consent. Written informed consent was obtained from the individual(s) for the publication of any potentially identifiable images or data included in this article.

## Author contributions

PH: Data curation, Formal analysis, Investigation, Resources, Software, Writing – original draft, Writing – review & editing, Conceptualization, Methodology, Validation. YY: Conceptualization, Investigation, Methodology, Project administration, Software, Supervision, Validation, Visualization, Writing – original draft, Writing – review & editing. C-TH: Data curation, Methodology, Visualization, Writing – review & editing. FZ: Data curation, Validation, Visualization, Writing – review & editing. Y-KX: Data curation, Investigation, Supervision, Validation, Writing – review & editing. JY: Conceptualization, Data curation, Investigation, Resources, Software, Supervision, Visualization, Writing – review & editing. JX: Conceptualization, Funding acquisition, Investigation, Supervision, Validation, Writing – original draft, Writing – review & editing.

## Funding

The author(s) declare financial support was received for the research, authorship, and/or publication of this article. Ministry of Science and Technology of the People's Republic of China National Nature Science Foundation of China AWARD NUMBER 82271939.

## Conflict of interest

Authors YY and JY were employed by company Dianei Technology.

The remaining authors declare that the research was conducted in the absence of any commercial or financial relationships that could be construed as a potential conflict of interest.

## Publisher's note

All claims expressed in this article are solely those of the authors and do not necessarily represent those of their affiliated

organizations, or those of the publisher, the editors and the reviewers. Any product that may be evaluated in this article, or claim that may be made by its manufacturer, is not guaranteed or endorsed by the publisher.

## Supplementary material

The Supplementary Material for this article can be found online at: <https://www.frontiersin.org/articles/10.3389/fonc.2024.1464555/full#supplementary-material>

## References

- Singh D, Vignat J, Lorenzoni V, Eslahi M, Ginsburg O, Lauby-Secretan B, et al. Global estimates of incidence and mortality of cervical cancer in 2020: a baseline analysis of the WHO Global Cervical Cancer Elimination Initiative. *Lancet Global Health*. (2023) 11:e197–206. doi: 10.1016/S2214-109X(22)00501-0
- Ramalingam S-S, Vansteenkiste J, Planchard D, Cho BC, Gray JE, Ohe Y. Overall survival with osimertinib in untreated, EGFR-mutated advanced NSCLC. *N Engl J Med*. (2020) 382:41–50. doi: 10.1056/NEJMoa1913662
- Maemondo M, Inoue A, Kobayashi K, Sugawara S, Oizumi S, Isobe H. Gefitinib or chemotherapy for non-small-cell lung cancer with mutated EGFR. *N Engl J Med*. (2010) 362:2380–8. doi: 10.1056/NEJMoa0909530
- Liang W, Zhong R, He J. Osimertinib in EGFR-mutated lung cancer. *N Engl J Med*. (2021) 384:675. doi: 10.1056/NEJMc2033951
- Reguart N, Remon J. Common EGFR-mutated subgroups (Del19/L858R) in advanced non-small-cell lung cancer: chasing better outcomes with tyrosine kinase inhibitors. *Future Oncol*. (2015) 11:1245–57. doi: 10.2217/fon.15.15
- Wang S, Shi J, Ye Z, Dong D, Yu D, Zhou M. Predicting EGFR mutation status in lung adenocarcinoma on computed tomography image using deep learning. *Eur Respir J*. (2019) 53(3). doi: 10.1183/13993003.00986-2018
- Chen Z, Gao S, Ding C, Luo T, Xu J, Xu S. CT-based non-invasive identification of the most common gene mutation status in patients with non-small cell lung cancer. *Med Phys*. (2024) 51:1872–82. doi: 10.1002/mp.16744
- Song J, Ding C, Huang Q, Luo T, Xu X, Chen Z. Deep learning predicts epidermal growth factor receptor mutation subtypes in lung adenocarcinoma. *Med Phys*. (2021) 48:7891–9. doi: 10.1002/mp.v48.12
- Li S, Ding C, Zhang H, Song J, Wu L. Radiomics for the prediction of EGFR mutation subtypes in non-small cell lung cancer. *Med Phys*. (2019) 46:4545–52. doi: 10.1002/mp.v46.10
- Kawazoe Y, Shiinoki T, Fujimoto K, Yuasa Y, Hirano T, Matsunaga K. Comparison of the radiomics-based predictive models using machine learning and nomogram for epidermal growth factor receptor mutation status and subtypes in lung adenocarcinoma. *Phys Eng Sci Med*. (2023) 46:395–403. doi: 10.1007/s13246-023-01232-9
- Schneider B-J. Non-small cell lung cancer staging: proposed revisions to the TNM system. *Cancer Imaging*. (2008) 8:181–5. doi: 10.1102/1470-7330.2008.0029
- Mahmoudian M, Venalainen M-S, Klen R, Elo LL. Stable iterative variable selection. *Bioinformatics*. (2021) 37:4810–7. doi: 10.1093/bioinformatics/btab501
- Liu Z, Mao H, Wu C-Y, Feichtenhofer C, Darrell T, Xie S. A convNet for the 2020s. *2022 IEEE/CVF Conference on Computer Vision and Pattern Recognition (CVPR)* (2022), 11966–76. doi: 10.1109/CVPR52688.2022.01167
- He K, Zhang X, Ren S, Sun J. Deep residual learning for image recognition. *2016 IEEE Conference on Computer Vision and Pattern Recognition (CVPR)* (2016), 770–8. doi: 10.1109/CVPR.2016.90
- Liu Z, Lin Y, Cao Y, Hu H, Wei Y, Zhang Z. Swin transformer: hierarchical vision transformer using shifted windows. *2021 IEEE/CVF International Conference on Computer Vision (ICCV)* (2021), 9992–10002. doi: 10.1109/ICCV48922.2021.00986
- Yang J, Huang X, He Y, Xu J, Yang C, Xu G. Reinventing 2D convolutions for 3D images. *IEEE J Biomed Health Inf*. (2021) 25:3009–18. doi: 10.1109/JBHI.2021.3049452
- Zhu W, Shen S, Zhang Z. Improved multiclassification of schizophrenia based on xgboost and information fusion for small datasets. *Comput Math Methods Med*. (2022) 2:0221581958. doi: 10.1155/2022/1581958
- Fluss R, Faraggi D, Reiser B. Estimation of the Youden Index and its associated cutoff point. *Biom J*. (2005) 47:458–72. doi: 10.1002/bimj.200410135
- Wang C, Xu X, Shao J, Zhou K, Zhao K, He Y. Deep learning to predict EGFR mutation and PD-L1 expression status in non-small-cell lung cancer on computed tomography images. *J Oncol*. (2021) 2021:5499385. doi: 10.1155/2021/5499385
- Liu G, Xu Z, Ge Y, Jiang B, Groen H, Vliegenthart R. 3D radiomics predicts EGFR mutation, exon-19 deletion and exon-21 L858R mutation in lung adenocarcinoma. *Transl Lung Cancer Res*. (2020) 9:1212–24. doi: 10.21037/tlcr-20-122
- Hayashi H, Nadal E, Gray J-E, Ardizzoni A, Caria N, Puri T. Overall treatment strategy for patients with metastatic NSCLC with activating EGFR mutations. *Clin Lung Cancer*. (2022) 23:e69–82. doi: 10.1016/j.clcc.2021.10.009
- Kang W, Qiu X, Luo Y, Luo J, Liu Y, Xi J. Application of radiomics-based multiomics combinations in the tumor microenvironment and cancer prognosis. *J Transl Med*. (2023) 21:598. doi: 10.1186/s12967-023-04437-4
- Cluceru J, Interian Y, Phillips J-J, Molinaro AM, Luks TL, Alcaide-Leon P. Improving the noninvasive classification of glioma genetic subtype with deep learning and diffusion-weighted imaging. *Neuro Oncol*. (2022) 24:639–52. doi: 10.1093/neuonc/noab238